Bicolor K-edge spectral photon-counting CT imaging for the diagnosis of thoracic endoleaks: A dynamic phantom study

Benoit Cosset, Monica Sigovan, Sara Boccalini, Fadi Farhat, Philippe Douek, Loic Boussel, Salim Aymeric Si-Mohamed

Diagnostic and Interventional Imaging 104 (2023) 235–242

Original article/Research, New developments & Artificial Intelligence

Bicolor K-edge spectral photon-counting CT imaging for the diagnosis of thoracic endoleaks: A dynamic phantom study

Benoit Cosset[a,b], Monica Sigovan[b], Sara Boccalini[b,c], Fadi Farhat[d], Philippe Douek[b,c], Loic Boussel[b,e], Salim Aymeric Si-Mohamed[b,c,*]

[a] *Department of Cardiovascular Surgery, Hôpital Louis Pradel, Hospices Civils de Lyon, 69500 Bron, France*
[b] *University Lyon, INSA-Lyon, Université Claude Bernard Lyon 1, UJM-Saint Etienne, CNRS, INSERM, CREATIS UMR 5220, U1206, F–69621, 69100 Villeurbanne, France*
[c] *Department of Radiology, Hôpital Louis Pradel, Hospices Civils de Lyon, 69500 Bron, France*
[d] *Department of Cardio-vascular Surgery, Infirmerie Protestante de Lyon, 69300 Caluire-et-Cuire, France*
[e] *Department of Radiology, Hôpital de la Croix Rousse, Hospices Civils de Lyon, 69500 Bron, France*

ARTICLE INFO

Keywords:
Contrast media
Endoleaks
Multidetector computed tomography
Photon-counting CT
Thoracic aorta

ABSTRACT

Purpose: The purpose of this study was to investigate the feasibility of identifying and characterizing the three most common types of endoleaks within a thoracic aorta aneurysm model using bicolor K-edge imaging with a spectral photon-counting computing tomography (SPCCT) system in combination with a biphasic contrast agent injection.

Materials and methods: Three types of thoracic endoleaks (type 1, 2 and 3) were created in a dynamic anthropomorphic thoracic aorta phantom. Protocol consisted in an injection of an iodinated contrast material followed 80 seconds after an injection of a gadolinium-based contrast agent (GBCA). The phantom was scanned using a clinical prototype SPCCT during bicolor phase imaging consisting in an early distribution of GBCA and a late distribution of iodine. Conventional and spectral images were reconstructed for differentiating between the contrast agents and measuring their respective attenuation values and concentrations inside and outside the stent graft.

Results: Conventional images failed to provide specific dynamic imaging contrast agents in the aneurysmal sac and outside the stent graft while spectral images differentiated their specific distribution. In type 1 and 3 thoracic endoleaks, GBCA concentration was measured outside the stent graft at 6.1 ± 3.7 (standard deviation [SD]) mg/mL and 6.0 ± 4.0 (SD) mg/mL, respectively, in favor of an early blood flow. In type 2 thoracic endoleak, iodine was measured outside the stent graft at 24.3 ± 5.5 (SD) mg/mL in favor of a late blood flow in the aneurysmal sac.

Conclusion: Bicolor K-edge imaging enabled SPCCT allows a bicolor characterization of thoracic aorta endoleaks in a single acquisition in combination with a biphasic contrast agent injection.

1. Introduction

Endoleak is a common complication of thoracic aorta endovascular aneurysm repair (EVAR) that can occur in 10 to 20% of patients [1]. They are characterized by the presence of blood flow between the aortic wall and the stent graft, and are classified into five types depending on their mechanism; of which, types 1, 2 and 3 are the most frequent ones [2]. Endoleaks can lead to aneurysm growth and sometimes rupture with, for example, an estimated 0.5–0.9% risk of rupture in the presence of a type 2 endoleak, explaining the recommendation for an early identification using conventional computed tomography (CT) and treatment using minimally invasive techniques [3]. However, conventional CT is limited by its inability to differentiate between contrast enhanced blood and highly attenuating materials often present in and nearby the aneurysm sac such as calcification, stent grafts or embolization materials (glue or ethylene vinyl alcohol copolymer) [4,5]. In addition, conventional CT does not provide a dynamic evaluation of the iodinated contrast material distribution, which limits the identification of the endoleak mechanism. Altogether, these limitations explain the need for a standard triphasic protocol to identify and characterize an endoleak. A triphasic protocol generally consists in an unenhanced phase followed by an arterial, and then a venous phase after intravenous administration of an

Abbreviations: CT, Computed tomography; ECMO, Extracorporeal membrane oxygenation; EVAR, Endovascular aortic repair; GBCA, Gadolinium-based contrast agent; PCD, Photon-counting detector; SD, Standard deviation; SPCCT, Spectral photon-counting computed tomography; T1, Monocolor phase; T2, Bicolor phase

* Corresponding author
E-mail address: salim.si-mohamed@chu-lyon.fr (S.A. Si-Mohamed).

https://doi.org/10.1016/j.diii.2022.12.003

iodinated contrast material [6]. Despite this standardized protocol, a substantial number of endoleaks are misdiagnosed, which highlights the need for improvement in CT imaging in this specific field [7].

Recently, new detectors with energy-resolving capabilities called photon-counting detectors (PCDs) have been implemented in CT systems enabling spectral capabilities. Contrary to conventional CT in which all the photon energies are integrated, the PCDs enable measurement of the energy of each photon and its classification within an energy window [8–11]. Spectral photon-counting CT (SPCCT) systems allow obtaining a decomposition of an image between different materials as a function of their proper attenuation, through mainly the K-edge imaging technique, which opens the door to monocolor and bicolor imaging capabilities [11,10]. Monocolor imaging is defined as the ability to differentiate one contrast agent from the surrounding tissue while bicolor allows a differentiation between two different atoms-based contrast agents. The perspective of such techniques is to take benefit from the specific identification of a contrast agent distribution within a tissue allowing new approaches in CT imaging such as molecular imaging [12,13]. In addition, bicolor imaging enables a simultaneous identification in a single acquisition of two contrast agents that by injecting them at a different time of injection may provide a dynamic evaluation of a tissue or cavity such as previously performed for the liver parenchyma imaging [14]. Altogether, SPCCT may hold great promises for improving the endoleak imaging by providing the advantages of the spectral imaging features.

The purpose of this study was to investigate the feasibility of identifying and characterizing the three most common types of endoleaks within a thoracic aorta aneurysm model using bicolor K-edge imaging with a SPCCT system in combination with a biphasic contrast agent injection.

2. Materials and methods

2.1. Thoracic aorta phantom

A synthetic human thoracic aorta, was constructed using a silicone rubber life-size model of a patient specific thoracic aorta aneurysm geometry using a three-dimensional printing technique (Fig. 1) [15]. The thoracic aorta model was fed by an extracorporeal membrane oxygenation (ECMO) with a speed of 2800 revolution per minutes (*i.e.*, a flow equal to 1.5 liter per minute). This flow represents approximately one-third of the cardiac outflow in an adult male of 70 kg. The main container was of six liters of water while in both ECMO lines, pump, filter and prosthesis, the volume was of two liters. A dilution of the contrast agent similar to the dilution of the contrast agent in the human body during clinical CT examination was obtained [16]. The proximal part of the aorta model was connected to the flow circuit. The distal part of the aorta model was divided in two ducts: one flowing in the main container and then going back to the ECMO and one flowing in the left subclavian artery. The duct connected the subclavian artery was used in endoleak type 2 for feeding the aneurysm through a collateral aortic branch.

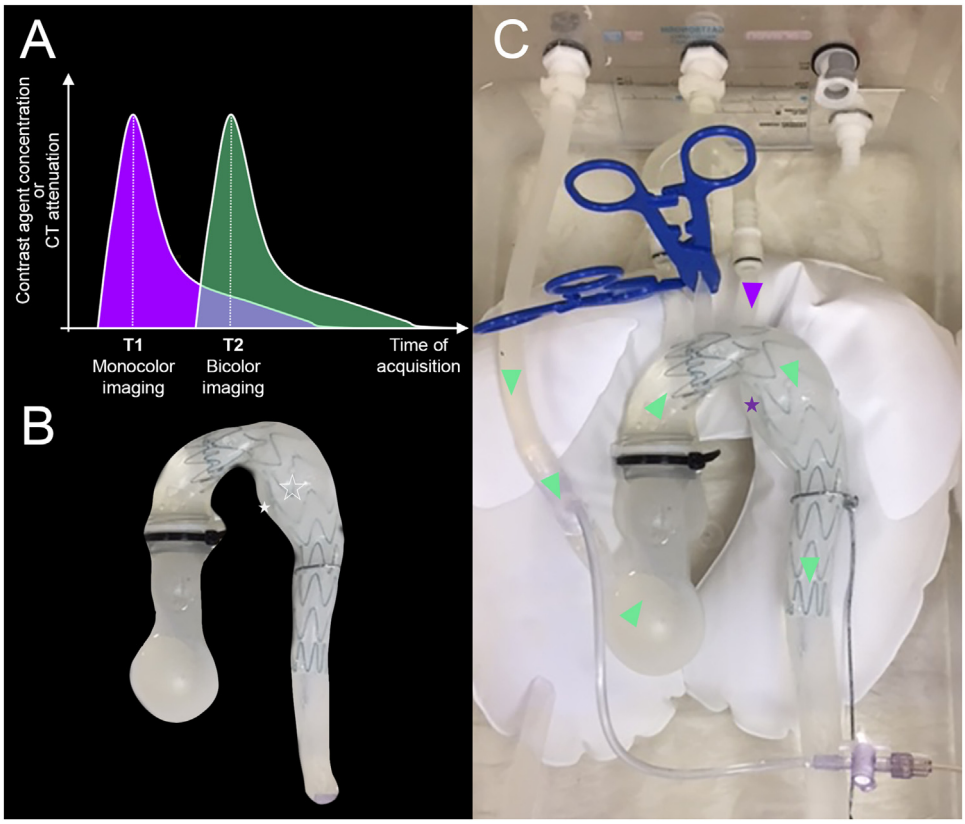

Fig. 1. Imaging and phantom characteristics. (A) Illustration of the contrast agent enhancement within the aortic lumen during monocolor (T1) and bicolor (T2) phases (purple indicates iodinated contrast agent; Green indicates gadolinium-based contrast agent). (B) Photograph of the aortic phantom model with visualization of the aneurysm sac (white star) and the aortic lumen (open star). (C) Complete phantom set-up with illustration of the contrast agent flow in a type 2 endoleak model (purple arrowheads indicate iodinated contrast agent; Green arrowheads indicate gadolinium-based contrast agent).

2.2. Endoleak models

A type 1 endoleak was created by implanting the graft (Valiant thoracic graft, Medtronic) from the isthmus to the descending aorta with a sufficient gap to allow a proximal endoleak. A type 2 endoleak was created by implanting the graft between the left carotid and the left subclavian artery, enabling a delayed flow from the subclavian artery into the aneurysm (Fig. 1). A type 3 endoleak was created by implanting a graft from the isthmus to the descending aorta and a second graft downstream the first one with a smaller diameter and a short overlap length.

2.3. Spectral photon-counting computed tomography

The SPCCT system was a clinical large field of view (50 cm in-plane) prototype system equipped with energy-sensitive PCD of 2-mm-thick cadmium zinc telluride with a pixel pitch of 270 × 270 μm^2 at isocenter, bonded to Philips' proprietary ChromAIX2 application-specific integrated circuit, relying on the direct conversion high band gap semiconductor of cadmium zinc telluride [17]. Each channel offered pulse-height discrimination with five controllable energy thresholds that were set at 30, 51, 62, 72, and 81 keV for optimized image quality on gadolinium-based contrast agent (GBCA) and iodine enhanced images [18]. Further technical details are described elsewhere [19,20].

2.4. Imaging protocol

Specific imaging of endoleaks was based on one helical acquisition of the aortic phantom during the bicolor phase (T2) (*i.e.*, after consecutive injections of an iodinated agent and a GBCA). An additional helical acquisition during the monocolor phase after an iodinated agent injection (T1) was performed for comparison purpose with imaging during T2. Acquisition parameters were a tube voltage of 120 kVp, a tube current of 100 mAs, a rotation time of 0.33 s and a pitch of 0.4. Conventional and spectral material decomposition images in water, iodine and gadolinium were reconstructed with a field-of-view of 220 mm, a matrix of 512 × 512 and a slice thickness of 0.5 mm, which corresponded to a voxel size of 0.43 × 0.43 × 0.50 mm^3.

2.5. Contrast agent protocol

A volume of 65 mL of an iodinated contrast agent (400 mg/mL, iomeprol, Iomeron®, Bracco Imaging) was injected at 5 mL/s preceding by 80 s a volume of 70 mL of a GBCA (0.5 M, gadoteridol, Prohance®, Bracco Imaging). Injection times were based on the clinical practice in order to simulate a venous enhancement of the aneurysm sac with the iodinated agent at T1 (representing the monocolor imaging phase, at 80 s), and an arterial enhancement with the GBCA at T2 (representing the bicolor imaging phase, at 15 s).

2.6. Image analysis

Regions-of-interest of more than 50 pixels were manually drawn by an experienced radiologist in cardiovascular imaging (S.A.S-M. with seven years of experience) inside the aortic lumen and the aneurysm 'sac on the conventional and spectral images (iodine and GBCA K-edge images). CT attenuation and concentrations of iodine and GBCA were measured in their respective images to evaluate the biodistribution of each agent and classify the endoleak type.

2.7. Statistical analysis

The normality of the distribution of quantitative variables was assessed using Shapiro-Wilk test. Quantitative variables were expressed as means ± standard deviations (SD) and ranges [21].

3. Results

3.1. Conventional CT images

During the monocolor phase (T1), conventional images showed high enhancement in the aortic lumen, as well as in the aneurysm sac in all the endoleaks with overall lower values than in the lumen. Similarly, during the bicolor phase (T2), enhancement was greater in the lumen than the sac for the types 1 and 3. In the type 2, enhancement was lower in the lumen than in the aneurysmal sac, indicating a possible accumulation of either one of the two contrast agents or both agents combined in the sac. For all conventional images, high densities arising from the stent graft were visible, limiting the assessment of the aneurysm sac and the quantification of CT attenuation due to strong streak artifacts (Figs. 2, 3, 4).

3.2. Bicolor spectral photon-counting CT images

3.2.1. Monocolor phase (T1) analysis

Similarly to the conventional CT images, a high concentration of iodine was observed within the aortic lumen and aneurysm sac. A lower concentration of iodine was observed in the aneurysm sac only in the type 2 endoleak. Gadolinium K-edge images did not show any signal in the lumen (Figs. 2–4). Only noise was measured with a mean value below to 1 mg/mL.

3.2.2. Bicolor phase (T2) analysis

In type 1 and 3 endoleaks, iodine images showed a moderate concentration of iodine within the aortic lumen and aneurysm sac. Gadolinium K-edge images showed a high concentration of GBCA in the aortic lumen and the aneurysm sac but in a lower magnitude in the aneurysm sac. These findings indicated the presence of a blood flow between the aortic lumen and the aneurysm sac during early enhancement phase on gadolinium K-edge images combined to a persistent delayed enhancement of the aneurysmal sac on iodine images. Altogether, these findings indicated either a type 1 or 3 endoleaks (Figs. 2 and 4).

In the type 2 endoleak, iodine images showed an 8-fold increase in concentration within the aneurysm sac than in the aortic lumen while the gadolinium K-edge images showed a high concentration of GBCA only in the lumen. These findings indicate first the absence of a blood flow between the aortic lumen and the aneurysm sac during early enhancement phase on gadolinium K-edge images combined to a delayed enhancement of the aneurysmal sac on iodine images. Altogether, these findings indicate a type 2 endoleak (Fig. 3).

Finally, gadolinium K-edge images did not show the stent graft, while it was visible on both conventional and iodine images. Quantitative results are reported in Table 1 and displayed in Fig. 5.

4. Discussion

In the present study, we demonstrated the feasibility of bicolor imaging enabled by SPCCT K-edge imaging in a dynamic aortic phantom for identifying the three most frequent types of endoleaks that can occur after thoracic EVAR. In addition, we used a biphasic protocol for contrast agent administration that enabled in only one acquisition obtaining dynamic information of the endoleak mechanism.

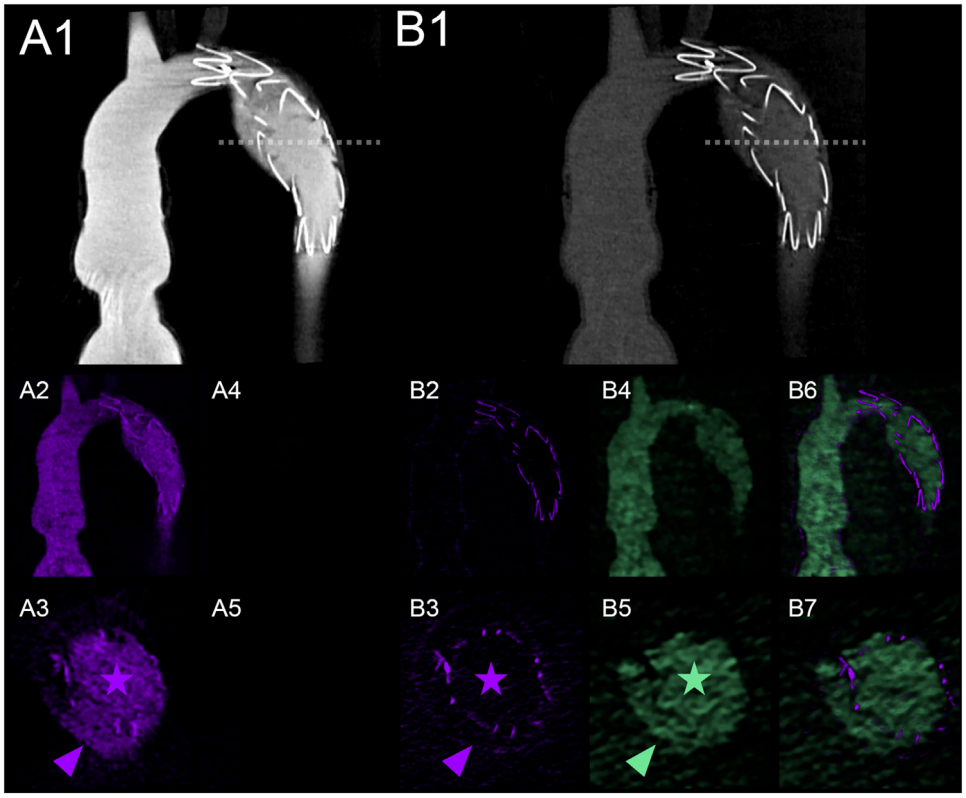

Fig. 2. Spectral photon counting computed tomography qualitative imaging of a type 1 endoleak during the monocolor (A1-A5) and bicolor (B1-B7) phases of enhancement on conventional CT (A1), spectral iodine (in purple) and gadolinium K-edge (in green) images. Enhancement in the aneurysm sac (purple arrowhead) and aortic lumen (purple star) is seen during the monocolor phase, such as on gadolinium K-edge image (green star and green arrowhead) during the bicolor phase indicating an early endoleak.

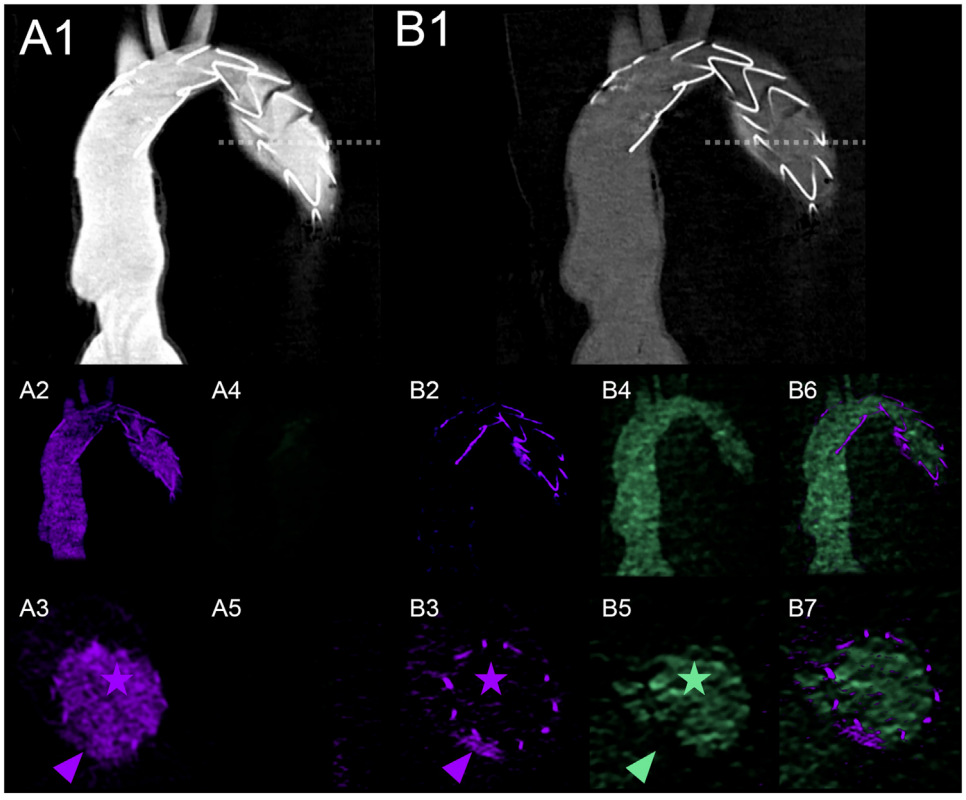

Fig. 3. Spectral photon counting computed tomography qualitative imaging of a type 2 endoleak during the monocolor (A1–A5) and bicolor (B1–B7) phases of enhancement on conventional CT (A1), spectral iodine (in purple) and gadolinium K-edge (in green) images. Enhancement in the aneurysm sac (purple arrowhead) and in the aortic lumen (purple star) is seen on iodine images during the monocolor phase while enhancement is only visible in the aortic lumen on gadolinium K-edge image (green star) during the bicolor phase. Instead, a high enhancement of iodine is seen in the aneurysm sac (purple arrowhead) during the bicolor phase indicating a delayed endoleak.

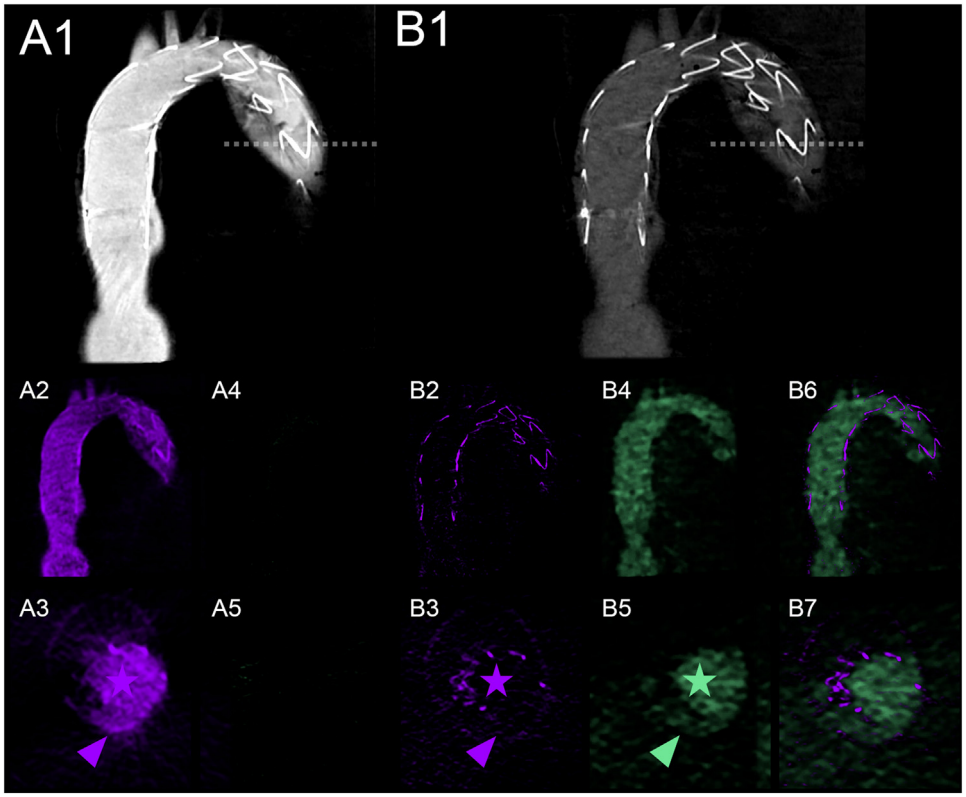

Fig. 4. Spectral photon counting computed tomography qualitative imaging of a type 3 endoleak during the monocolor (A1–A5) and bicolor (B1–B7) phases of enhancement on conventional CT (A1), spectral iodine (in purple) and gadolinium K-edge (in green) images. Enhancement in the aneurysm sac (purple arrowhead) and aortic lumen (purple star) is seen during the monocolor phase, such as on gadolinium K-edge image (green star and arrow) during the bicolor phase indicating an early endoleak.

Previously, Dangelmaier et al. have demonstrated in a static phantom that SPCCT K-edge imaging allowed the differentiation between iodinated contrast agents, GBCA and calcification [22]. But their phantom was only made of multiple cavities for simulating an axial portion of an aortic aneurysm and did not offer a dynamic evaluation of the blood flow [22]. In addition, the SPCCT system used in their study allowed only a field-of-view of 16 cm as well as a time of rotation of 0.5 s, which are technical limitation for Human imaging. In the present study, a clinical SPCCT prototype with a large field-of-view of 50 cm and time of rotation of 0.33 s was used with which Human studies have been performed, indicating a potential for human translation [9,19,20,23–26]. While conventional images failed to provide dynamic information in the aortic model, spectral images through K-edge imaging allowed informing on the dynamic enhancement of the aortic lumen and aneurysm sac. For type 1 and 3 endoleaks, iodine and gadolinium K-edge images showed similar quantitative and qualitative distribution both in the aortic lumen and aneurysm sac during the bicolor phase. This is explained by a large communication

Table 1
Results of the quantitative analysis performed in the aortic lumen and aneurysm sac during monocolor (T1) and bicolor (T2) phases.

Endoleak type	Phase	Region of interest	Attenuation (HU)	Iodine concentration (mg/mL)	Gadolinium concentration (mg/mL)
1	T1	Aortic lumen	741 ± 35 [701–768]	36.6 ± 4.5 [32–41]	N/A
		Aneurysm sac	556 ± 110 [458–675]*	27.7 ± 12.4 [20–42]*	N/A
		Background	29 ± 7.5 [24–38]	1.7 2.1 [0.1–4.2]	0.7 ± 1.1 [−0.7–1.4]
	T2	Aortic lumen	353 ± 39 [314–392]	3.1 ± 2.0 [2–5]	8.3 ± 3.8 [4.5–12.1]
		Aneurysm sac	258 ± 50 [208–308]*	1 ± 4.5 [−3.5–5.5]**	6.1 ± 3.7 [2.4–9.8]*
		Background	30 ± 3.3 [27–34]	1.0 ± 0.8 [0.3–2.2]	0.8 ± 0.8 [−0.2–1.8]
2	T1	Aortic lumen	730 ± 40 [690–780]	36.7 ± 3.5 [33–41]	N/A
		Aneurysm sac	522 ± 27 [490–550]*	10.2 ± 1.2 [33–41]**	N/A
		Background	37 ± 11 [29–53]	0.3 ± 0.1 [0.2–0.8]	0.9 ± 0.2 [0.7–1.2]
	T2	Aortic lumen	344 ± 36 [308–380]	2.3 ± 4.9 [−2.2–5.8]	4.7 ± 7.2 [−3.3–10.5]
		Aneurysm sac	540 ± 39 [501–579]*	24.3 ± 5.5 [18.8–19.8]**	0.3 ± 3.2 [−2.9–3.5]**
		Background	34 ± 2.6 [31–37]	0.4 ± 0.1 [0.3–0.6]	0.8 ± 0.1 [0.7–1]
3	T1	Aortic lumen	753 ± 42 [711–790]	35 ± 3.1 [31–38]	N/A
		Aneurysm sac	499 ± 120 [353–599]*	22.4 ± 9.9 [11.6–32]*	N/A
		Background	23 ± 5.4 [19–31]	0.3 ± 0.2 [0.1–0.7]	1.1 ± 0.2 [0.9–1.4]
	T2	Aortic lumen	313 ± 33 [280–346]	2.5 ± 5 [−2.3–7.7]	7.3 ± 3.8 [3.5–11.1]
		Aneurysm sac	258 ± 42 [216–300]*	2.7 ± 4.5 [−1.8–7.2]*	6 ± 4 [2–10] *
		Background	35 ± 3.1 [33–40]	0.1 ± 1.0 [0.1–0.3]	0.9 ± 0.5 [0.4–1.6]

Variables are expressed as means ± standard deviations; numbers in brackets are ranges.
* Indicates a variation in CT attenuation or concentration of contrast agents in the aneurysm sac by comparison with the aortic lumen. One symbol (*) indicates a variation < 50%. Two symbols (**) indicate a variation > 50%. HU = Hounsfield unit.
N/A indicates that no value was measured because of the absence of GBCA injected during the monocolor phase (T1).

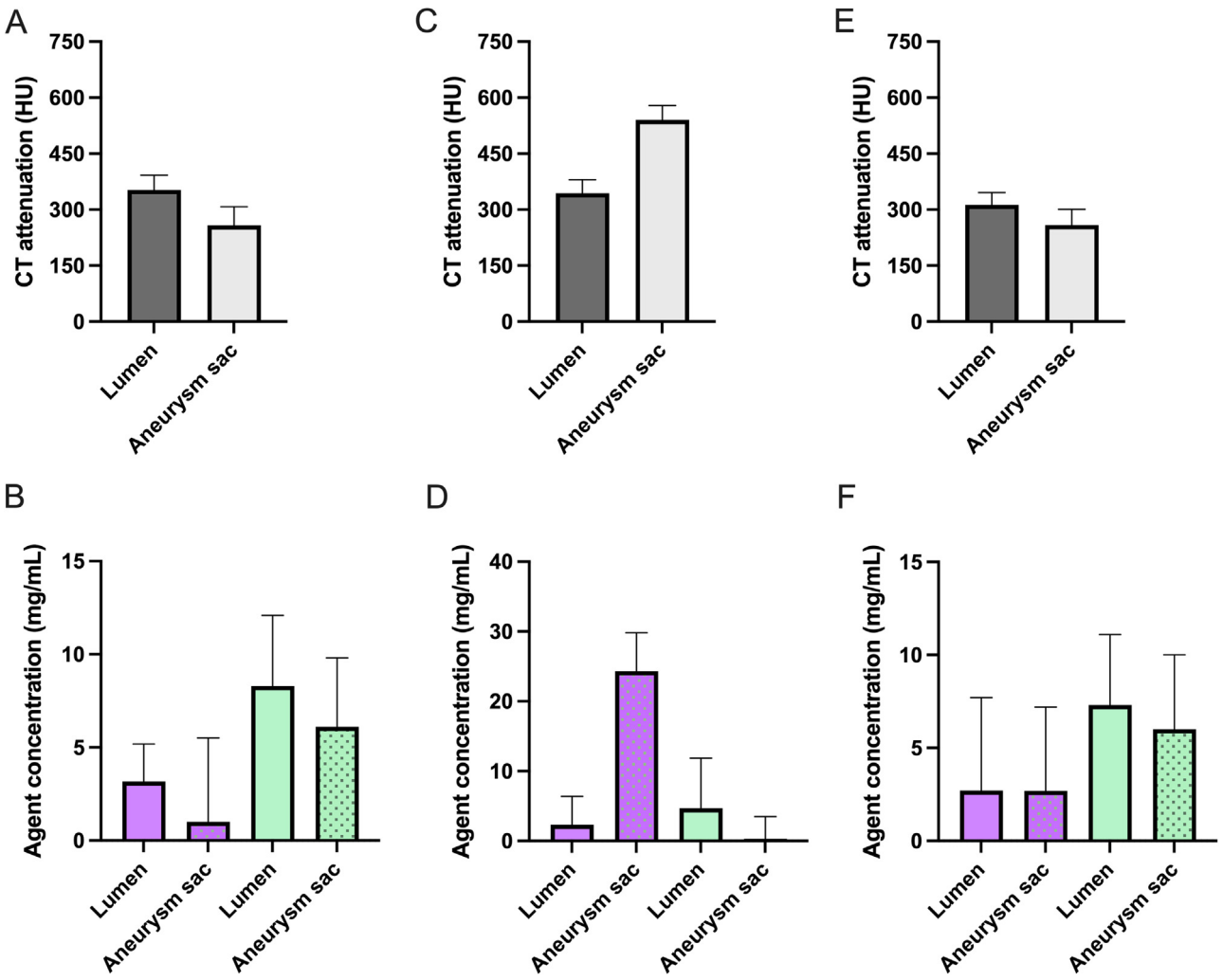

Fig. 5. Graphs show spectral photon counting computed tomography quantitative analysis of type 1 (A–B), 2 (C–D) and 3 (E–F) endoleaks during the bicolor phase (T2) of enhancement on conventional CT (A, C, E), spectral iodine (in purple; B, D, F) and gadolinium K-edge (in green; B, D, F) images. Differences in CT attenuation values between the lumen and aneurysm sac are lower with conventional CT by comparion with those obtained with spectral images, which allows the identification and characterization of each endoleak type.

with the aneurysm sac, such as created experimentally. It is noteworthy to mention that for type 1 endoleak, concentration of iodine during the bicolor phase was lower in the aneurysm sac than in the aortic lumen. This finding is probably a marker of a faster clearance of the agent from the aneurysm sac than what was found in type 3, explaining the faster flow in the aneurysm sac for type 1, as shown with time resolved CT [27]. For type 2 endoleak, iodine and gadolinium K-edge maps demonstrated a delayed enhancement in the aneurysm sac. This is explained by the delayed flow in the afferent subclavian vessel created experimentally. In addition, as shown on the GBCA-enhanced images during the bicolor phase, no early flow was observable, which is expected in type 2.

The present study provides one more evidence of the capabilities of bicolor imaging for improving the current CT protocols. First, it allows providing in one acquisition a dynamic evaluation of a tissue enhancement. In the same line, Si-Mohamed et al. have provided evidence for simultaneous evaluation of a liver arterial phase using a GBCA and a liver portal phase using an iodinated contrast agent [14]. Second, it allows decreasing the ionization radiation burden by suppressing the need for a triphasic protocol. This is particularly of concern in patients followed for an endovascular aortic treatment, as demonstrated by Kalef-Ezra et al. who found a median cumulative radiation dose of 62 mSv in the first year following abdominal EVAR [28]. Third, bicolor imaging allows avoiding spatial misregistration caused by patient motion and breathing between each phase of the protocol particularly within the aneurysm sac which would be of great interest for automatic detection and measurement of endoleaks using machine learning methods for example [29]. Even if motion correction and post-processing techniques are available, the suppression of this issue would increase spatial resolution particularly needed for endoleak task imaging. Altogether, these evidences are highlighting the strengths of bicolor imaging. Nevertheless, one strong limitation should be noted. Use of two contrast agents simultaneously in vivo should be carefully evaluated as well as the cumulative volume of agents injected. The main limitation is the volume of GBCA needed for reaching the current sensitivity threshold of K-edge imaging, that is strongly limited by the noise as highlighted in the present study [11,30]. However, sensitivity is expected to be improved in a near future with further noise handling algorithms such as with regularized iterative methods during the material decomposition process [31], during the reconstruction process [32] or in a one-step algorithm that would embed both process [33]. Another strong advantage of SPCCT relies in the improvement in spatial resolution achieved by the PCDs, which is particularly of interest for vascular and stent imaging [34,35]. As an example, Boccalini et al. demonstrated in human that SPCCT enabled a greater coronary intrastent delineation and a lowering of blooming and beam hardening artefacts in comparison to a conventional dual-layer CT [26]. In the same line, Si-Mohamed et al. showed that SPCCT enabled in a greater conspicuity and sharpness of coronary calcifications in human, with

an expected improvement of the image quality for all the patients [20]. Hence, SPCCT is holding great promises for endoleak imaging either due to its spatial resolution or spectral capabilities such as showed in the present study.

Our study has limitations. First, we did not implant calcium within the aortic phantom. Nevertheless, previous studies have shown ability of SPPCT to distinguish between calcium and contrast agent [12,13, 36, 37]. Indeed, with a K-edge energy equal to 50.2 Kev, gadolinium map excludes calcium elements (*i.e.*, K-edge energy equal to 4.03 Kev). Two acquisitions were performed. The purpose was to have a fair comparison between the bicolor GBCA distribution and the monocolor iodine distribution. Nevertheless, by showing similar distribution between those, our observations showed that only one SPCCT is needed. Iodine concentrations during the monocolor phase were greater than GBCA ones during the bicolor phase. Nevertheless, this was expected due to higher atom load injected using an iodinated agent concentration of 400 mg/mL by comparison with a GBCA concentration of 78 mg/mL. This highlights a limitation for the use of current contrast agents with CT and suggests that the development of GBCA suitable for SPCCT imaging is needed.

In conclusion, SPCCT allows identifying three most frequent types of thoracic endoleaks in a dynamic model of thoracic aorta aneurysm. Bicolor imaging enabled by SPCCT K-edge imaging, provides dynamic enhancement of the aortic lumen and aneurysm sac in only one acquisition that allows characterizing the endoleak types.

Declaration of Competing Interest

The authors has no conflicts of interest to disclose in relation with this article.

CRediT authorship contribution statement

Benoit Cosset: Conceptualization, Methodology, Formal analysis, Investigation, Writing – original draft. **Monica Sigovan:** Writing – review & editing. **Sara Boccalini:** Writing – review & editing. **Fadi Farhat:** Writing – review & editing. **Philippe Douek:** Resources, Writing – review & editing, Project administration, Funding acquisition. **Loic Boussel:** Methodology, Software, Validation, Resources, Writing – review & editing, Supervision. **Salim Aymeric Si-Mohamed:** Conceptualization, Methodology, Validation, Formal analysis, Investigation, Data curation, Writing – original draft, Supervision.

Acknowledgment

We thank Adja Diaw, Mohammad Varasteh, Angèle Houmeau, Marjorie Villien, Franck Lavenne, Jean-Baptiste Langlois and Caroline Bouillot for their support during the experiments.

Human rights

Not applicable for phantom studies.

Informed consent and patient details

Not applicable for phantom studies.

Funding information

This work was supported by European Union Horizon 2020 grant No 643694.

Author contributions

All authors attest that they meet the current International Committee of Medical Journal Editors (ICMJE) criteria for Authorship.

References

[1] Thrumurthy SG, Karthikesalingam A, Patterson BO, Holt PJE, Hinchliffe RJ, Loftus IM, et al. A systematic review of mid-term outcomes of thoracic endovascular repair (TEVAR) of chronic type B aortic dissection. Eur J Vasc Endovasc Surg 2011;42:632–47.
[2] White GH, Yu W, May J, Chaufour X, Stephen MS. Endoleak as a complication of endoluminal grafting of abdominal aortic aneurysms: classification, incidence, diagnosis, and management. J Endovasc Surg 1997;4:152–68.
[3] Marcelin C, Le Bras Y, Petitpierre F, Midy D, Ducasse E, Grenier N, et al. Safety and efficacy of embolization using Onyx® of persistent type II endoleaks after abdominal endovascular aneurysm repair. Diagn Interv Imaging 2017;98:491–7.
[4] Golzarian J, Dussaussois L, Abada HT, Gevenois PA, Van Gansbeke D, Ferreira J, et al. Helical CT of aorta after endoluminal stent-graft therapy: value of biphasic acquisition. AJR Am J Roentgenol 1998;171:329–31.
[5] Macari M, Chandarana H, Schmidt B, Lee J, Lamparello P, Babb J. Abdominal aortic aneurysm: can the arterial phase at CT evaluation after endovascular repair be eliminated to reduce radiation dose? Radiology 2006;241:908–14.
[6] Partovi S, Trischman T, Rafailidis V, Ganguli S, Rengier F, Goerne H, et al. Multimodality imaging assessment of endoleaks post-endovascular aortic repair. Br J Radiol 2018;91:20180013.
[7] van der Laan MJ, Bartels LW, Viergever MA, Blankensteijn JD. Computed tomography versus magnetic resonance imaging of endoleaks after EVAR. Eur J Vasc Endovasc Surg 2006;32:361–5.
[8] Si-Mohamed S, Bar-Ness D, Sigovan M, Cormode DP, Coulon P, Coche E, et al. Review of an initial experience with an experimental spectral photon-counting computed tomography system. Nucl Instrum Methods Phys Res Sect A 2017;873:27–35.
[9] Si-Mohamed SA, Miailhes J, Rodesch PA, Boccalini S, Lacombe H, Leitman V, et al. Spectral photon-counting CT technology in chest imaging. J Clin Med 2021;10:5757.
[10] Greffier J, Villani N, Defez D, Dabli D, Si-Mohamed S. Spectral CT imaging: technical principles of dual-energy CT and multi-energy photon-counting CT. Diagn Interv Imaging 2022. doi: 10.1016/j.diii.2022.11.003.
[11] Si-Mohamed S, Bar-Ness D, Sigovan M, Tatard-Leitman V, Cormode DP, Naha PC, et al. Multicolour imaging with spectral photon-counting CT: a phantom study. Eur Radiol Exp 2018;2:34.
[12] Si-Mohamed S, Cormode DP, Bar-Ness D, Sigovan M, Naha PC, Langlois J-B, et al. Evaluation of spectral photon counting computed tomography K-edge imaging for determination of gold nanoparticle biodistribution in vivo. Nanoscale 2017;9:18246–57.
[13] Si-Mohamed SA, Sigovan M, Hsu JC, Tatard-Leitman V, Chalabreysse L, Naha PC, et al. In vivo molecular K-edge imaging of atherosclerotic plaque using photon-counting CT. Radiology 2021;300:98–107.
[14] Si-Mohamed S, Tatard-Leitman V, Laugerette A, Sigovan M, Pfeiffer D, Rummeny EJ, et al. Spectral photon-counting computed tomography (SPCCT): in-vivo single-acquisition multi-phase liver imaging with a dual contrast agent protocol. Sci Rep 2019;9:8458.
[15] Attia C, Abdulrazzaq S, Huet L, Saint-James H, Beuf O, Farhat F, et al. Feasibility of stent-graft placement with real-time MR fluoroscopy in a nonrigid aortic phantom. J Vasc Interv Radiol 2008;19:1354–60.
[16] Nadler SB, Hidalgo JH, Bloch T. Prediction of blood volume in normal human adults. Surgery 1962;51:224–32.
[17] Steadman R, Herrmann C, Livne A. ChromAIX2: a large area, high count-rate energy-resolving photon counting ASIC for a spectral CT prototype. Nucl Instrum Methods Phys Res Sect A 2017;862:18–24.
[18] Alvarez RE. Estimator for photon counting energy selective x-ray imaging with multibin pulse height analysis. Med Phys 2011;38:2324–34.
[19] Si-Mohamed S, Boccalini S, Rodesch PA, Dessouky R, Lahoud E, Broussaud T, et al. Feasibility of lung imaging with a large field-of-view spectral photon-counting CT system. Diagn Interv Imaging 2021;102:305–12.
[20] Si-Mohamed SA, Boccalini S, Lacombe H, Diaw A, Varasteh M, Rodesch PA, et al. Coronary CT angiography with photon-counting CT: first-in-human results. Radiology 2022;302:303–13.
[21] Barat M, Jannot AS, Dohan A, Soyer P. How to report and compare quantitative variables in a radiology article. Diagn Interv Imaging 2022;103:571–3.
[22] Dangelmaier J, Bar-Ness D, Daerr H, Muenzel D, Si-Mohamed S, Ehn S, et al. Experimental feasibility of spectral photon-counting computed tomography with two contrast agents for the detection of endoleaks following endovascular aortic repair. Eur Radiol 2018;28:3318–25.
[23] Boccalini S, Si-Mohamed S, Dessouky R, Sigovan M, Boussel L, Douek P. Feasibility of human vascular imaging of the neck with a large field-of-view spectral photon-counting CT system. Diagn Interv Imaging 2021;102:329–32.
[24] Jungblut L, Abel F, Nakhostin D, Mergen V, Sartoretti T, Euler A, et al. Impact of photon-counting-detector-CT derived virtual-monoenergetic-images and iodine-maps on the diagnosis of pleural empyema. Diagn Interv Imaging 2022. doi: 10.1016/j.diii.2022.09.006.

[25] Boccalini S, Si-Mohamed S. Spectral photon counting CT: not just a pimped-up new version of dual-energy CT. Diagn Interv Imaging 2022. doi: 10.1016/j.diii.2022.10.009.
[26] Boccalini S, Si-Mohamed SA, Lacombe H, Diaw A, Varasteh M, Rodesch P-A, et al. First in-human results of computed tomography angiography for coronary stent assessment with a spectral photon counting computed tomography. Invest Radiol 2022;57:212–21.
[27] Sommer WH, Becker CR, Haack M, Rubin GD, Weidenhagen R, Schwarz F, et al. Time-resolved CT angiography for the detection and classification of endoleaks. Radiology 2012;263:917–26.
[28] Kalef-Ezra JA, Karavasilis S, Ziogas D, Dristiliaris D, Michalis LK, Matsagas M. Radiation burden of patients undergoing endovascular abdominal aortic aneurysm repair. J Vasc Surg 2009;49:283–7.
[29] Hahn S, Perry M, Morris CS, Wshah S, Bertges DJ. Machine deep learning accurately detects endoleak after endovascular abdominal aortic aneurysm repair. JVS Vasc Sci 2020;1:5–12.
[30] Kim J, Bar-Ness D, Si-Mohamed S, Coulon P, Blevis I, Douek P, et al. Assessment of candidate elements for development of spectral photon-counting CT specific contrast agents. Sci Rep 2018;8:12119.
[31] Ducros N, Abascal JFP-J, Sixou B, Rit S, Peyrin F. Regularization of nonlinear decomposition of spectral x-ray projection images. Med Phys 2017;44:e174–87.
[32] Sawatzky A, Xu Q, Schirra C, Anastasio M. Proximal ADMM for multi-channel image reconstruction in spectral X-ray CT. IEEE Trans Med Imaging 2014;3:1657–68.
[33] Mory C, Sixou B, Si-Mohamed S, Boussel L, Rit S. Comparison of five one-step reconstruction algorithms for spectral CT. Phys Med Biol 2018;63:235001.
[34] Sigovan M, Si-Mohamed S, Bar-Ness D, Mitchell J, Langlois J-B, Coulon P, et al. Feasibility of improving vascular imaging in the presence of metallic stents using spectral photon counting CT and K-edge imaging. Sci Rep 2019;9:19850.
[35] Bratke G, Hickethier T, Bar-Ness D, Bunck AC, Maintz D, Pahn G, et al. Spectral photon-counting computed tomography for coronary stent imaging: evaluation of the potential clinical impact for the delineation of in-stent restenosis. Invest Radiol 2020;55:61–7.
[36] Riederer I, Si-Mohamed S, Ehn S, Bar-Ness D, Noël PB, Fingerle AA, et al. Differentiation between blood and iodine in a bovine brain: initial experience with spectral photon-counting computed tomography (SPCCT). PloS One 2019;14:e0212679.
[37] Si-Mohamed S, Thivolet A, Bonnot P-E, Bar-Ness D, Képénékian V, Cormode DP, et al. Improved peritoneal cavity and abdominal organ Imaging using a biphasic contrast agent protocol and spectral photon counting computed tomography K-edge imaging. Invest Radiol 2018;53:629–39.